



Published in final edited form as:

*Glia*. 2016 February ; 64(2): 214–226. doi:10.1002/glia.22924.

## Gap junction coupling confers isopotentiality on astrocyte syncytium

Baofeng Ma<sup>1</sup>, Richard Buckalew<sup>2</sup>, Yixing Du<sup>1</sup>, Conrad M. Kiyoshi<sup>1</sup>, Catherine C. Alford<sup>1</sup>, Wei Wang<sup>1,#</sup>, Dana D. McTigue<sup>1</sup>, John J. Enyeart<sup>1</sup>, David Terman<sup>3</sup>, and Min Zhou<sup>1,\*</sup>

<sup>1</sup>Department of Neuroscience, The Ohio State University Wexner Medical Center, Columbus, OH 43210, USA

<sup>2</sup>Mathematical Biosciences Institute, The Ohio State University, Columbus, OH 43210, USA

<sup>3</sup>Department of Mathematics, The Ohio State University, Columbus, OH 43210, USA

### Abstract

Astrocytes are extensively coupled through gap junctions into a syncytium. However, the basic role of this major brain network remains largely unknown. Using electrophysiological and computational modeling methods, we demonstrate that the membrane potential ( $V_M$ ) of an individual astrocyte in a hippocampal syncytium, but not in a single, freshly isolated cell preparation, can be well-maintained at quasi-physiological levels when recorded with reduced or  $K^+$  free pipette solutions that alter the  $K^+$  equilibrium potential to non-physiological voltages. We show that an astrocyte's associated syncytium provides powerful electrical coupling, together with ionic coupling at a lesser extent, that equalizes the astrocyte's  $V_M$  to levels comparable to its neighbors. Functionally, this minimizes  $V_M$  depolarization attributable to elevated levels of local extracellular  $K^+$  and thereby maintains a sustained driving force for highly efficient  $K^+$  uptake. Thus, gap junction coupling functions to achieve isopotentiality in astrocytic networks, whereby a constant extracellular environment can be powerfully maintained for crucial functions of neural circuits.

### Keywords

Electrical coupling; Coupling coefficient; Membrane potential;  $K^+$  clearance

### Introduction

Establishment of a syncytium through gap junction coupling is a prominent feature of astrocytes in the central nervous system (Brightman and Reese 1969; Dermietzel and Spray 1993; Giaume et al. 2010; Ransom 1996). Gap junction coupling is known to mediate the

\*Correspondence: Min Zhou, 4066C Graves Hall, 333 West 10th Avenue, Columbus, OH 43210, Phone: (614) 366-9406, Fax: (614) 688-8742, zhou.787@osu.edu.

#Present address: Department of Physiology, Tongji Medical College, Huazhong University of Science and Technology, Wuhan, Hubei 430030, China.

**Author contribution:** B.M. and M.Z. designed experiments; B.M. and Y.D. performed experiments; D.D.M. contributed the transgenic mice; B.M., R.B., D.T and J.J.E. performed theoretical analysis; B.M., J.J.E., R.B., D.T. and M.Z. wrote the manuscript. All authors discussed the results and commented on the manuscript.

exchange of small molecules ( $< \sim 1.2$  kDa). This facilitates important homeostatic and signaling functions of astrocytes, such as spatial buffering of  $K^+$  and  $Na^+$  ions and the long-range redistribution of nutrients, metabolites and signaling molecules for the coordination of neuronal activity and brain energy metabolism (Kuga et al. 2011; Langer et al. 2012; Lin et al. 1998; Newman 2001; Orkand et al. 1966; Rose and Ransom 1997; Rouach et al. 2008; Simard et al. 2003; Wang et al. 2012).

Gap junctions also enable electrical coupling to minimize membrane potential ( $V_M$ ) differences among interconnected cells in a mutual and rapid manner. For pairs of coupled cells, the strength of electrical coupling, termed the coupling coefficient (CC), is commonly evaluated by the ratio of voltage in coupled to that of injected cell (transjunctional voltage to input voltage) using the dual patch recording method. However, the coupling coefficient between any two nearest neighboring astrocytes in the intact brain has been a long-standing but unresolved question. Although the transjunctional voltage analysis has been used to explore this question between astrocytes (Ceelen et al. 2001; Kettenmann and Ransom 1988; Meme et al. 2009; Ransom and Kettenmann 1990; Xu et al. 2010), the coupling coefficient cannot be accurately measured due to an extremely low membrane resistance that shunts the experimentally injected currents through astrocyte's low resistance membrane ( $\sim 6$  M $\Omega$ ) (Ma et al. 2014). At the syncytial level, each hippocampal astrocyte is directly coupled with 11 nearest neighbors and several hundreds of astrocytes are coupled in a syncytium (D'Ambrosio et al. 1998; Xu et al. 2010), an intriguing question is how the aggregate coupling strength affects the  $V_M$  and other physiological behavior of any individual astrocyte in a syncytium. No methodology is, as yet, available to tackle these fundamentally important questions.

In the present study, we combine electrophysiological and computational modeling methods to investigate the mechanisms by which nearest neighboring astrocytes coordinate the  $V_M$ 's in a syncytium. The study is conceived based on a basic feature of astrocytes: they behave as perfect  $K^+$  electrodes as a result of their predominant expression of leak type  $K^+$  conductances (Kuffler et al. 1966; Ransom and Goldring 1973). Therefore, one can experimentally lower the intracellular  $K^+$  concentration ( $[K^+]_i$ ) using reduced or  $K^+$ -free pipette solutions to establish a depolarized  $K^+$  equilibrium potential ( $E_K$ ) in a recorded astrocyte to levels that can be predicted by the membrane equilibrium potential ( $E_M$ ) from the Goldman-Hodgkin-Katz (GHK) equation. The nearest neighbors should then act to hyperpolarize the recorded astrocyte by minimizing the differences in  $K^+$  concentrations (ionic coupling) and membrane potential (electrical coupling). Consequently, the deviation of measured  $V_M$  from the experimentally established  $E_M$  in the recorded astrocyte can serve as a reliable indicator of the coupling strength among astrocytes in a syncytium (See mathematic modeling). We hypothesized that a strong gap junction coupling among hippocampal CA1 astrocytes suppresses the  $V_M$  depolarization in recordings made with reduced or free  $K^+$  pipette solutions.

## Materials and Methods

### Animals

The C57/BL6 mice of both genders older than P21 (Charles River), and PDGFRA-driven eGFP transgenic mice (Hesp et al. 2015) were used in the present study according to the guidelines of the Institutional Animal Care and Use Committee, The Ohio State University.

### Hippocampal slice preparation

For slice recording, hippocampal slices were prepared as described previously (Ma et al. 2014). In brief, after anesthesia with 8% chloral hydrate in 0.9% NaCl, the mouse brain was rapidly removed from skull and submerged into ice-cold oxygenated (95% O<sub>2</sub> /5% CO<sub>2</sub>) cutting solution containing (in mM): 125 NaCl, 3.5 KCl, 25 NaHCO<sub>3</sub>, 1.25 NaH<sub>2</sub>PO<sub>4</sub>, 0.1 CaCl<sub>2</sub>, 3 MgCl<sub>2</sub>, and 10 glucose. Coronal hippocampal slices (250 μm) were cut at 4°C with a Vibratome (Pelco 1500) and transferred to the normal aCSF (in mM): 125 NaCl, 3.5 KCl, 25 NaHCO<sub>3</sub>, 1.25 NaH<sub>2</sub>PO<sub>4</sub>, 2 CaCl<sub>2</sub>, 1 MgCl<sub>2</sub>, and 10 glucose (osmolality, 295 ± 5 mOsm; pH 7.3–7.4) at room temperature (20–22°C). Slices were kept in aCSF with continuous oxygenation for at least 1 hour before recording.

### Sulforhodamine 101 Staining

For sulforhodamine 101 (SR101, Invitrogen, New York, NY) staining (Nimmerjahn et al. 2004), the slices were transferred to a slice-holding basket containing 0.6 μM SR101 in aCSF at 34 °C for 30 min. Then, the basket was transferred back to the normal aCSF at room temperature before the experiment.

### Fresh dissociation of hippocampal tissues

At the animal age older than P21, the spatially distinct domains, electrical coupling, and K<sup>+</sup> channel expression have all reached maturity (Bushong et al. 2004; Xu et al. 2010; Zhou et al. 2006). To dissociate single and multiple astrocytes with intact domain and functional gap junctional coupling, a new hippocampal tissue dissociation method was used (Du et al. 2015). Briefly, after incubation with SR-101 for 30 min, the CA1 regions were dissected out from slices and cut into small pieces (1 mm<sup>2</sup>), then placed in oxygenated aCSF containing 24U/ml papain and 0.8 mg/ml L-cysteine for 7 min. After papain digestion, a fire polished glass pipette, diameter ~150 μm, was used to triturate the loosened tissues 5–7 times into a tissue suspension, and then transferred into the recording chamber. The dissociated cells were allowed 3–5 min to touch down to the bottom of the chamber before switching on a constant aCSF perfusion at flow rate of 2 ml/min. The viable astrocytes, with their elaborate processes and well-preserved domain shape, are similar to their counterparts *in situ* (Figures 2A–B).

### Electrophysiology

To record astrocytes in CA1 *stratum radium*, individual slices were transferred to a recording chamber (RC-22, Warner Instruments, Holliston, MA) mounted on a Olympus BX51WI microscope equipped with infrared differential interference (IR-DIC) and were perfused with oxygenated aCSF (2.5 mM/min) at room temperature.

Astrocytes *in situ* were identified based on SR101 staining; they typically exhibited an irregular soma shape, diameter around 10  $\mu\text{m}$ , with several visible primary processes stemming from the soma. The NG2 glial cells were identified by GFP from PDGFRA-driven eGFP transgenic mice (Hesp et al. 2015). The interneurons were identified based on their large soma size and shapes. After establishing whole-cell configuration, the mature astrocytes were unequivocally identified by their expression of passive membrane  $\text{K}^+$  conductance (Zhou et al. 2006). Interneurons expressed large inward  $\text{Na}^+$  currents in voltage clamp recording and fired action potentials spontaneously when switched to current clamp recording (Figure 1F).

Recording pipettes were fabricated from borosilicate capillaries (1.5/0.86 mm outer/inner diameter, Warner Instruments, Holliston, MA) using a Flaming/Brown Micropipette Puller (Model P-87, Sutter Instrument). When filled with pipette solution noted below, the pipettes had the open tip resistance of 2.5–3.5  $\text{M}\Omega$ . The standard pipette solution contained (in mM): 140 KCl or Kgluconate, 0.5  $\text{CaCl}_2$ , 1  $\text{MgCl}_2$ , 5 EDTA, 10 HEPES, 3  $\text{Mg}^{2+}$ -ATP and 0.3  $\text{Na}^+$ -GTP that was titrated with KOH to pH 7.25–7.27. The final osmolality was 280 mOsm. The 140 mM KCl was substituted by NaCl, or NMDGCl either partially or fully in the referred experiments.

Whole-cell membrane current or membrane potential was amplified by MultiClamp 700A or MultiClamp 700B amplifiers, and the data acquisition was controlled by pClamp 9.2 (Molecular Devices, Sunnyvale, CA) installed on Dell personal computers. DIGIDATA 1322A interface was used to convert digital-analog signals between amplifier and computer. A minimum of 2  $\text{G}\Omega$  seal resistance was required before rupturing the membrane for whole-cell configuration. The total membrane resistance, or input resistance ( $R_{\text{in}}$ ), was measured by using the “Membrane test” protocol built into the pClampex. The access resistance ( $R_{\text{a}}$ ) was not compensated for in all the voltage clamp recordings for low  $R_{\text{M}}$  astrocytes (Ma et al. 2014). The membrane potential ( $V_{\text{M}}$ ) was read either in “I = 0” mode or measured directly in current clamp mode with no holding currents. Astrocytes with a resting membrane potential more positive than  $-70$  mV in both brain slices and freshly isolated single astrocytes were discarded. All the experiments were conducted at room temperature ( $20 \pm 2^\circ\text{C}$ ). The liquid junction potential was compensated for before establishment of cell-attached mode in all the recordings and confirmed to be  $\sim 0$  mV after experiments by withdrawal of recording pipette.

SR101 positive staining was used to confirm the astrocytic identity and determine the number of astrocytes in a freshly dissociated tissue block. The same patch clamp set-up and procedure, for slice astrocyte recording, was used for freshly dissociated astrocyte recording.

In the experiment for manipulating coupling strength, brain slices were pretreated with aCSF containing 100  $\mu\text{M}$  meclofenamic acid (MFA) for one hour before recording and perfused with the same solution during recording. When  $V_{\text{M}}$  was stable, 100  $\mu\text{M}$  MFA plus 100  $\mu\text{M}$   $\text{Ba}^{2+}$  was bath applied. In the experiment for determining effect of 100  $\mu\text{M}$  MFA + 100  $\mu\text{M}$   $\text{Ba}^{2+}$  on the  $R_{\text{M}}$ , dual patch recording was used as we previous reported (Ma et al. 2014).

## Local high K<sup>+</sup> application

We used VC<sup>3</sup>4 Controller (ALA Scientific Instruments) for focal high K<sup>+</sup> application (pressure 6 psi). Focal high K<sup>+</sup> (23.5 mM) or aCSF was delivered via a pipette to the recorded cell ~10 μm away from soma, and 100 μM SR-101 was included in the application solutions to visualize and measure the areas affected by focally applied high K<sup>+</sup>. Software provided by ALA Scientific Instruments was used for programming of the durations of high K<sup>+</sup> application.

## Imaging capture

Confocal images were obtained using a Zeiss LSM 510 at the Hunt-Curtis Imaging Facility. A fluorescent imaging system (Polychrome V system from Till Photonics, Germany) is used for Epifluorescence imaging and high resolution visualization of small glial soma and placing of dual patch pipettes on it. This system was used for identifying astrocyte based on SR101 positive staining (Fig. 1A and Fig. 2B), and for simultaneous dual patch.

## Statistical analysis

Data are reported as mean ± SEM. Mean differences between groups were using *t* test or two-way ANOVAs followed by *post hoc* testing when main effect was significant at *p* < 0.05. Data were analyzed using Origin 11 software package (OriginLab, Northampton, MA).

## Results

### Syncytial Coupling Equalizes the Membrane Potential among Astrocytes in the Network

To test our hypothesis, we identified astrocytes based on SR101 staining from the hippocampal CA1 region (10) and recorded  $V_M$  under current clamp mode. In control experiments, we used patch pipette solution containing 140 mM K<sup>+</sup> (K<sup>+</sup>-based solution, [K<sup>+</sup>]<sub>p</sub>) (Fig. 1A and B). In cell-attached mode, the gigaohm seal formation led to an anticipated  $V_M$  shift from 0 mV to  $-38.1 \pm 18.5$  mV (*n* = 13) for the low membrane resistance astrocytes (Supp. Info. Fig. 1). The breakthrough of the membrane patch shifted the  $V_M$  immediately to a resting membrane potential of  $-78.1 \pm 0.7$  mV (*n* = 11) (Fig. 1B), as expected for cells almost exclusively permeable to K<sup>+</sup> (17).

When similar recordings were made with patch pipettes in which the [K<sup>+</sup>]<sub>i</sub> was reduced from 140 mM to 70 mM by substitution with Na<sup>+</sup>, the recorded  $V_M$  was essentially unchanged ( $-78.1 \pm 1.1$  mV, *n* = 6) (Fig. 1G) and differed significantly from the GHK predicted 11.1 mV depolarization. Furthermore, the GHK equation predicts a 105 mV depolarization if pipette K<sup>+</sup> is totally substituted by Na<sup>+</sup> (Na<sup>+</sup>-based solution, [Na<sup>+</sup>]<sub>p</sub>). However, Na<sup>+</sup>-based solution depolarized the cells only by 4.5 mV ( $-73.5 \pm 0.9$  mV, *n* = 10), compared to the control astrocytes (Fig. 1C and G). In all recordings with reduced or K<sup>+</sup>-free pipette solutions, the recorded  $V_M$  remained at a steady-state level during a recording time of ~ 10 min. In some recordings, we purposely extended time to over one hour, and the steady-state  $V_M$  remained unchanged, indicating gap junction coupling provided a sustained  $V_M$  control over recorded astrocytes. These results support the hypothesis that there exists a powerful gap junction coupling among CA1 astrocytes *in situ* (Supp. Info. Fig. 2).

To determine if a similar  $V_M$  behavior occurs in other uncoupled cells in this brain region (Xu et al. 2014), we used  $\text{Na}^+$ -based pipette solution to record NG2 glia in hippocampal slices prepared from PDGF $\alpha$ 1-driven-GFP transgenic mice (Fig. 1D)(Hesp et al. 2015); NG2 glia are known to also function as  $\text{K}^+$  electrodes (Maldonado et al. 2013). NG2 glia followed the GHK prediction by depolarizing rapidly to a stable  $V_M$  level of  $7.3 \pm 1.9$  mV ( $n = 9$ ,  $P < 0.01$ ) (Fig. 1E and G). Likewise, uncoupled CA1 interneurons also depolarized to  $1.3 \pm 0.7$  mV ( $n = 5$ ) when recorded with  $\text{Na}^+$ -based pipette solution (Fig. 1F and G).

To ensure that such “anomalous”  $V_M$  behavior was not specific to  $\text{Na}^+$  ions, we replaced  $\text{K}^+$  either partially or fully with NMDG $^+$ . Substitution of NMDG $^+$  for  $\text{K}^+$  resulted in  $V_M$  changes similar to those observed from  $\text{Na}^+$  substitution (Fig. 1H). Thus, syncytial coupling suppresses the  $V_M$  depolarization that is expected for an uncoupled single astrocyte recorded after a full substitution of intracellular  $\text{K}^+$  by  $\text{Na}^+$  or NMDG.

To confirm that gap junction coupling was responsible for the equalization of  $V_M$  in astrocytes, we pre-incubated the brain slices with 100  $\mu\text{M}$  meclofenamic acid (MFA) for 1 hour to block the gap junction coupling (Xu et al. 2010). Under this condition, the  $\text{Na}^+$ -based solution depolarized astrocytes to a steady-state  $V_M$  of  $-13.9 \pm 1.8$  mV ( $n = 10$ ) in MFA (Fig. 1I). The computational model predicts that this corresponds to a 99.3% inhibition of coupling strength ( $s = \text{coupling conductance} / \text{membrane conductance of nearest neighbors}$ ) with MFA (Supp. Info. Fig. 4). To confirm this prediction, 100  $\mu\text{M}$   $\text{Ba}^{2+}$  was applied to inhibit a major astrocyte  $\text{K}^+$  channel, Kir4.1. This increased the membrane resistance,  $R_M$ , from the control  $6.3 \pm 0.7$  M $\Omega$  to  $18.4 \pm 4.4$  M $\Omega$  ( $n = 7$ ), corresponding to a 2.9-fold increase in the coupling strength and a predicted  $V_M$  hyperpolarization to  $-23.9$  mV (Supp. Info. Fig. 4). Consistent with this prediction, the astrocyte  $V_M$  hyperpolarized to  $-23.4 \pm 2.7$  mV ( $n = 10$ ) in the presence of 100  $\mu\text{M}$   $\text{Ba}^{2+}$  in MFA aCSF (Fig. 1I and J). Thus gap junction coupling is responsible for the mildly altered astrocyte  $V_M$  recorded with MFA and a  $\text{Na}^+$ -based pipette solution *in situ*. Moreover, the experimental results validated the mathematical model we have developed for this study.

### Larger Syncytia have Stronger Control over an individual Astrocyte's $V_M$

The computational model predicts that if the number of cells that are coupled to the recorded cell with  $\text{Na}^+$ -based electrode solution is increased, then the recorded  $V_M$  will lie closer to the physiological  $E_M$  of the nearest neighbors (Supp. Info. Fig. 2). To test this prediction, we used freshly isolated hippocampal tissues that contained single to multiple astrocytes with their spatially distinct domains and functional  $\text{K}^+$  channels well-maintained (Du et al. 2015) (Fig. 2A). A  $\text{Na}^+$ -based pipette solution was used to record astrocytes located in the center of the tissues. As the number of cells in the syncytium that were coupled to the recorded cell increased, so did the deviation of the recorded  $V_M$  from the GHK predicted value for a  $\text{Na}^+$ -based pipette solution (Fig. 2C–F and K). Thus, the number of neighboring astrocytes has an aggregate effect in suppressing the  $V_M$  depolarization induced by  $\text{Na}^+$ -loading in the recorded astrocyte (Supp. Info. Fig. 2).

In single astrocytes, the same  $\text{Na}^+$ -based pipette solution induced an initial hyperpolarization, reflecting the undisturbed initial  $[\text{K}^+]_i$ , followed by a depolarization to  $-0.02 \pm 0.74$  mV ( $n = 12$ ), as predicted by the GHK equation (Fig. 2G). A subsequent bath

application of elevated 23.5 mM  $K^+$  also induced a predicted  $V_M$  depolarization (Fig. 2H). When switching to voltage-clamp recordings, the depolarization induced outward currents were almost fully eliminated due to the absence of intracellular  $K^+$  ion (Fig. 2I left). Removal of the 3.5 mM  $K^+$  in the bath solution ( $[K^+]_e$ ) further abolished the inward currents (Fig. 2I middle), and the inward currents reemerged when 3.5 mM  $[K^+]_e$  was restored (Fig. 2I right). In contrast, the breakthrough of the membrane patch with  $K^+$ -base pipette solution shifted the  $V_M$  to the anticipated resting  $V_M$  of  $-78.4 \pm 1.9$  mV ( $n = 11$ ) in single astrocytes (Fig. 2J), which was comparable with astrocytes in slices (Fig. 1G). Thus, independent of which pipette solution was used, single astrocytes behave as a perfect  $K^+$  electrode.

### Contribution of Ionic Coupling in Maintaining the Astrocyte $V_M$ in situ

In astrocyte recordings with  $Na^+$ -based solution *in situ*, the  $K^+$ -mediated outward currents remained unchanged (Fig. 3A), suggesting the presence of  $K^+$  conducting ions in the recorded cell due to ionic coupling with the associated syncytium.

To determine how efficient gap junctions are in permitting ion exchange between coupled astrocytes, we used  $Na^+$ -based pipette solution to compare the time required for the full substitution of intracellular  $K^+$  in a freshly dissociated, single astrocyte with the time required in a pair of coupled astrocytes (doublet) (Fig. 3B). In both cases, a complete substitution of the endogenous  $K^+$  by  $Na^+$  from the pipette was indicated by the depolarization of  $V_M$  from its resting value to  $\sim 0$  mV, as predicted by the GHK equation. The computational modeling predicts that the high ion exchange efficacy enables a doublet to replace all the endogenous  $K^+$  by pipette  $Na^+$  with a time course similar to that of a single astrocyte (Fig. 3C,  $s = 1$ ). Let  $T_{50}$  be the half time for  $V_M$  to reach 0 mV. Then the ion exchange efficacy at the gap junctions can be estimated by computing the difference between the  $T_{50}$ 's in single and doublet astrocytes (Fig. 3C). The  $T_{50}$  was  $\sim 12$  times slower in doublets ( $4.67 \pm 0.36$  min,  $n = 5$ ) than that of single astrocytes ( $0.39 \pm 0.25$  min,  $n = 3$ ) (Fig. 3D–E). Thus, because of its relatively slow kinetics (see Supp. Info. Fig. 5 for further modeling analysis), ionic coupling is unlikely to be the major factor in maintaining a constant astrocyte  $V_M$  *in situ* (Fig. 1C, G and H).

### A Strong Electrical Coupling Confers Isopotentiality to Coupled Astrocytes

Electrical coupling is able to instantaneously equilibrates the  $V_M$ 's of coupled neurons (Connors and Long 2004). To examine the strength of electrical coupling and the level of  $V_M$  equilibration in coupled astrocytes, we considered a doublet in which the  $E_M$ 's of the two astrocytes were experimentally set up at sharply different levels. In dual patch recordings, a  $K^+$ -based pipette (P1) was sealed on one of the astrocytes, while a  $Na^+$ -based pipette (P2) was sealed on the other astrocyte (Fig. 4A1). The membrane of the astrocyte with the  $K^+$ -based electrode was ruptured first to measure the resting  $V_M$  of the doublet (Fig. 4A1); this did not interfere with the intercellular  $K^+$  concentration,  $[K^+]_i$ . The subsequent breakthrough of P2 initiated a  $Na^+$  influx and a re-equilibration of  $[K^+]_i$  and  $[Na^+]_i$  in the recorded doublet. Consistent with the ion exchange  $T_{50}$  at doublet gap junctions (Fig. 3D), the computational model predicts that  $[K^+]_i$  and  $[Na^+]_i$  should reach their new steady-state levels within 120 seconds (Fig. 4A2). There is then an intracellular  $[K^+]_i$  gradient from 140

mM at P1 to 0 mM  $K^+$  at P2. This corresponds to  $E_M$  equal to  $-74$  mV and  $-10$  mV at the respective pipettes (Fig. 4A2).

Despite a rapid separation between the battery potentials ( $E_M$ ) of P1 and P2, the breakthrough of P2 resulted in an instantaneous equilibration of the  $V_M$ 's to comparable levels at both pipettes (left inset, Fig. 4B). A strong electrical coupling was evident by the closely matched  $V_M$  amplitudes in the two cells as they depolarized in parallel towards their new steady-state levels (middle inset, Fig. 4B).

To examine the similarity between the dynamics of doublets and single astrocytes, we repeated the same experiment in single astrocytes (Fig. 4A3). The breakthrough of the P2 resulted in a pattern of  $V_M$  equilibration similar to that observed in doublets (Fig. 4C, and right inset). The  $V_M$  trajectories, in single and doublet astrocytes, all reached steady-state levels with comparable time courses (Fig. 4B–C). To quantify their similarities, we fitted a single exponential to each  $V_M$  depolarization, starting at the time of breakthrough of P2. The resulting time constants ( $\tau$ ) and depolarization amplitudes ( $A$ ) are comparable in all four pipettes (Fig. 4D), indicating that doublets behave electrically as one single astrocyte. The time constants in doublets were also similar to the  $T_{50}$  of single astrocytes (Fig. 3D–E). This indicates that  $Na^+$  influx predominantly replaced the endogenous  $K^+$  in the P2 attached cell; moreover, the cross-diffusion of  $Na^+$  and  $K^+$  across the gap junction was minimal in coupled doublets, as predicted by the computational model (Fig. 4A2 and S6). These results demonstrate that a powerful electrical coupling equilibrates the  $V_M$ 's of coupled astrocytes to a comparable level.

To directly estimate the gap junction coupling resistance in doublets, we replaced all  $K^+$  by  $Na^+$  in the recording solutions (Fig. 2I and 4E). This allows for maximal reduction in current shunting through the low resistance membrane. Under this condition, current injection in one astrocyte induced almost the same  $V_M$  shift in both astrocytes with a calculated coupling coefficient (CC) of  $94.3 \pm 3.2\%$  ( $n = 3$ ) (Fig. 4F), and a coupling resistance ( $R_g$ ) of  $4.2 \pm 1.5$   $M\Omega$  ( $n = 3$ , pair distance  $30.5 \pm 3.1$   $\mu m$ ) (Bennett 1966). As the  $R_g$  appeared to be even lower than the  $R_M$  of single astrocytes (Du et al. 2015), this suggested that, with maximally reduced current shunting, doublets should behave as single astrocytes in voltage clamp recordings (Supp. Info. Fig. 3, Table 2). To test this, a command voltage was delivered to P1 and the  $V_M$  shift in P2 was measured in current clamp (Fig. 4G). Consistently, the  $V_M$  shift in P2 followed the command voltages closely,  $V_M/V_c = 91.4 \pm 1.0\%$  ( $n = 3$ ) (Fig. 4G). These results demonstrate that the physical barrier between coupled astrocytes is almost absent electrically; therefore, equilibration of  $V_M$  among coupled astrocytes to an isopotential can be readily achieved so that doublets act as a single astrocyte.

### Syncytial Isopotentiality Facilitates $K^+$ Uptake under a Sustained Driving Force

The syncytial isopotential suggests that an anticipated regional  $V_M$  depolarization, in response, for example, to a local increase in extracellular  $K^+$  ( $[K^+]_e$ ) around a subdomain area of a single astrocyte, can be minimized. For a local  $[K^+]_e$  increase from 3.5 mM to 23.5 mM, the GHK equation predicts a 43.2 mV depolarization, whereas under isopotential conditions, the numerically predicted depolarization is approximately 5 mV (Supp. Info. Fig. 7).

We tested this prediction by comparing the high  $[K^+]_e$  responses from astrocytes and uncoupled NG2 glia *in situ*; both of these glial subtypes function similarly as  $K^+$  electrodes (Kuffler et al. 1966; Maldonado et al. 2013). We first bath applied 23.5 mM high  $K^+$  to maximally depolarize all the coupled astrocytes and NG2 glia *in situ*. The astrocytes and NG2 glia responded to high  $[K^+]_e$  with comparable time courses and maximum  $V_M$  amplitudes: astrocytes  $43.4 \pm 1.0$  mV ( $n = 7$ ) vs. NG2 glia  $42.8 \pm 1.1$  mV ( $n = 4$ ). These values followed the GHK prediction closely (Fig. 5A–B).

To simulate locally elevated  $[K^+]_e$  near a subdomain area of an astrocyte or an NG2 glia, we puffer applied 23.5 mM  $[K^+]_e$  through a patch pipette to the recorded cells (Fig. 5C). The high  $[K^+]_e$  affected area was monitored by SR101 fluorescence included in the solution. A 5 ms, high  $K^+$  puff affected an area with a diameter of  $26.4 \pm 0.3$   $\mu\text{m}$  ( $n = 4$ ) around the patched cells; this was less than a typical 50  $\mu\text{m}$  astrocytic domain (Bushong et al. 2002; Xu et al. 2014) (Fig. 5C). The high  $[K^+]_e$  puffer induced depolarization was significantly less in astrocytes ( $3.86 \pm 0.48$  mV,  $n = 4$ ) than in NG2 glia ( $12.13 \pm 0.66$  mV,  $n = 4$ ) (Fig. 5B–D). Puff aCSF alone did not alter the  $V_M$  (Fig. 5B). The significantly reduced  $V_M$  depolarization in astrocytes was very close to 5 mV, as predicted by the computational model (Supp. Info. Fig. 7). Thus, syncytial coupling is able to minimize local high  $[K^+]_e$  -induced  $V_M$  depolarization.

Because single astrocytes behave as perfect  $K^+$  electrodes, one expects that, at steady state,  $V_M$  lies very close to  $E_M$  and the  $K^+$  uptake driving force ( $V_M - E_M$ ) is negligible. If a single astrocyte is presented with a local increase in  $[K^+]_e$ , then a significant  $K^+$  driving force arises only transiently, as  $V_M$  rapidly depolarizes towards the newly established  $E_M$  (Fig. 5E). However, individual astrocytes within a syncytium are able to maintain a constant, nonzero driving force. This is because, as we have demonstrated, the  $V_M$  of an individual astrocyte is held nearly constant by the syncytial isopotential. Therefore, the  $K^+$  uptake driving force can be maintained until locally elevated  $[K^+]_e$  is completely taken up by the astrocytes (Supp. Info. Fig. 7). Thus, the syncytial isopotential transforms a “restricted local  $K^+$  uptake” model in a single astrocyte to a “sustained local  $K^+$  uptake” model in coupled astrocytes (Fig. 5E).

## DISUSSION

Neuronal and glial gap junction coupling was discovered sequentially over 50 years ago (Furshpan and Potter 1957; Kuffler and Potter 1964). While the discovery of the former immediately led to the notion of “electrical synapse” underlying one of the neuronal synaptic transmission mechanism, the electrical role of gap junctions in glial cells is still poorly defined (Ransom 1996). To answer this fundamental question, a novel experimental design has been conceived based a basic electrophysiological property of astrocytes; they behave as  $K^+$  electrode (Kuffler et al. 1966; Ransom and Goldring 1973). To examine this issue directly from native astrocytes, freshly dissociated hippocampal tissue has been used as new model (Du et al. 2015). To guide experimental design, predict and explain the experimental results, a computational modeling has been developed in this study.

### Astrocyte gap junction coupling functions to achieve syncytial isopotentiality

The following insights into astrocytic syncytium have been revealed. First, a surprisingly low gap junction coupling resistance ( $R_g$ , 4.2 M $\Omega$ ) and high coupling coefficient (94%) have been found in pairs of coupled astrocytes. This coupling coefficient is 2.1-folds higher than that of cultured astrocytes (44%) (Kettenmann and Ransom 1988; Ransom and Kettenmann 1990), and the  $R_g$  is even lower than astrocyte's membrane resistance ( $R_M$ , ~ 6.4 M $\Omega$ ) (Du et al. 2015). The strong electrical coupling enables any pair of neighboring astrocytes to immediately equilibrates their membrane potentials to closely matched levels and thus electrically behave as a single astrocyte. Second, at the syncytial level, strong electrical and ionic coupling equalizes the membrane potentials among coupled astrocytes to achieve syncytial isopotentiality. Astrocytes ensheath neuronal circuits throughout the brain, and maintain a homeostatic interstitial environment that is crucial for neuronal signaling and information processing. A new insight into this function is that the homeostatic support is achieved through a coordinated action of astrocytes governed by gap junction coupling established syncytial isopotentiality.

It has been speculated that a potential role of gap junction is to “clamp” neighboring astrocytes to an identical resting membrane potential, or syncytial isopotentiality, which could be essential for the maintenance of a uniform extracellular ion concentration (Muller 1996). In the present study, for the first time we have experimentally demonstrated that gap junction coupling confers isopotentiality on astrocyte syncytium. This finding is supported by an early *in vivo* observation from cat cortex: during interictal discharge the recorded glial cell  $V_M$  remained relatively stable although the amplitude of extracellular  $K^+$  concentration varied dramatically (Futamachi and Pedley 1976), suggesting that isopotentiality should also function physiologically *in vivo*.

### Syncytial Isopotentiality Facilitates $K^+$ Clearance

In this study, a demonstrated function of syncytial isopotentiality is to minimize the anticipated high  $[K^+]_e$ -induced membrane potential depolarization around a local area in the network, whereby a sustained  $K^+$  uptake driving force can be maintained for a higher  $K^+$  clearance efficiency (Fig. 5H). This observation has a significant implication for the frequently discussed “ $K^+$  spatial buffering” hypothesis.

The  $K^+$  spatial buffering hypothesis was proposed by Orkand et al (Orkand et al. 1966). Evidence that glial cells do utilize this mechanism for  $K^+$  clearance came from experiments performed in Müller cells (Newman 1984; Newman et al. 1984; Oakley et al. 1992), where a single Müller cell, a specialized astrocyte in retina, spatially transported  $K^+$  from the plexiform layers to the vitreous body, blood vessels and subretinal space, a mechanism termed “ $K^+$  siphoning”. Now increasing evidence indicates that this ‘spatial dependent’  $K^+$  clearance mechanism may work as well in syncytial coupled astrocytes (Coles et al. 1986; Gardner-Medwin and Nicholson 1983; Holthoff and Witte 2000; Kofuji et al. 2000; Wallraff et al. 2006). In the present study, we have demonstrated that syncytial isopotentiality makes  $K^+$  uptake more efficient. As demonstrated in this study, syncytial isopotentiality minimizes the local high  $[K^+]_e$ -induced  $V_M$  depolarization, and this maintains a sustained driving forces for  $K^+$  uptake. By extension, syncytial isopotentiality also increases the driving force

for  $K^+$  release in distant regions where  $[K^+]_e$  remains at the physiological level. Additionally, increase in both driving forces creates a maximum driving force for intracellular  $K^+$  transfer from high  $[K^+]_e$  region to remote regions with normal  $[K^+]_e$ . Therefore, syncytial isopotentiality facilitates all three critical steps in “ $K^+$  spatial buffering”,  $K^+$  uptake, intercellular transfer and release (Kofuji and Newman 2004).

### **Number of Nearest Neighbors and Coupling Strength Collectively Determine the Capacity of $K^+$ Clearance**

Previously, we have shown that each hippocampal astrocyte couples directly with 11 the nearest neighbors (Xu et al. 2014), Here we show that a strong coupling mediated syncytial isopotentiality facilitates the capacity of  $K^+$  uptake to level that could not be appreciated in the past. These observations, however, also rise an important physiological question. That is, whether and how the capacity of  $K^+$  clearance is determined by these two parameters?

This fundamental question can now be answered by modeling simulations (Supp. Info. Fig. 7). First, when coupling number keeps as a constant, the coupling strength ( $s$ ) determines the slope, or how fast, the high  $[K^+]_e$  can be brought back to the physiological levels. Second, when the coupling strength ( $s$ ) keeps as a constant, the number of coupling cells determines how close the final  $[K^+]_e$  can approach to the physiological  $[K^+]_e$  level. Third, when the coupling strength ( $s$ ) is sets at 1, as demonstrated in this study, the total capacity of  $K^+$  uptake can no longer increase with further increased number of nearest neighbors over 11. Thus the combination of these anatomic and physiological features is likely achieved over the course of evolution for the optimal function of astrocytes in the brain.

### **Future Studies**

The precise role of astrocytes in the adult brain remains to be defined (Nedergaard et al. 2003). An emerging view from this study is that astrocytes work as a team and the basic physiological function is achieved at syncytial network levels. This sheds new lights on future astrocyte study and urges more study to examine the functions achieved at syncytial (or system) levels.

Astrocyte coupling is important for equalization of intracellular  $Na^+$  concentration (Langer et al. 2012; Rose and Ransom 1997), calcium signaling and wave propagation (Khakh and McCarthy 2015; Kuga et al. 2011), and regulatory redistribution of glucose toward to active neurons in demand (Rouach et al. 2008). Meanwhile, there is an increasing awareness of astrocytes diversity (Giaume and Liu 2012; Zhang and Barres 2010). Thus, the experimental approach demonstrated in this study provides a powerful functional measurement to determine in the future the extent the syncytial isopotentiality exists in other brain regions and whether and how this crucial network function could be altered in various pathological disorders.

Additionally, the numerously expressed  $Na^+$ -dependent uptake systems (Cahoy et al. 2008; Kimelberg 2010) should be appreciated and reappraised with the consideration of syncytial isopotential. The present study also emphasizes the importance of homeostatic support as a basic astrocyte function in the brain.

## Supplementary Material

Refer to Web version on PubMed Central for supplementary material.

## Acknowledgments

This work was sponsored by grants from National Institute of Neurological Disorders and Stroke (RO1NS062784 to MZ, RO1NS043246 to DDM), a start-up fund from The Ohio State University College of Medicine (to MZ) and grants from the National Science Foundation (DMS 1410935 to DT and DMS 0931642 to the Mathematical Biosciences Institute). We thank Drs. Harold K. Kimelberg and Maiken Nedergaard for critical comments on the manuscript. We thank Dr. Bruce R. Ransom for providing insightful comments and suggestions for manuscript improvement during revision.

## References

- Bennett MV. Physiology of electrotonic junctions. *Ann N Y Acad Sci.* 1966; 137:509–39. [PubMed: 5229812]
- Brightman MW, Reese TS. Junctions between intimately apposed cell membranes in the vertebrate brain. *J Cell Biol.* 1969; 40:648–77. [PubMed: 5765759]
- Bushong EA, Martone ME, Ellisman MH. Maturation of astrocyte morphology and the establishment of astrocyte domains during postnatal hippocampal development. *Int J Dev Neurosci.* 2004; 22:73–86. [PubMed: 15036382]
- Bushong EA, Martone ME, Jones YZ, Ellisman MH. Protoplasmic astrocytes in CA1 stratum radiatum occupy separate anatomical domains. *J Neurosci.* 2002; 22:183–92. [PubMed: 11756501]
- Cahoy JD, Emery B, Kaushal A, Foo LC, Zamanian JL, Christopherson KS, Xing Y, Lubischer JL, Krieg PA, Krupenko SA, et al. A transcriptome database for astrocytes, neurons, and oligodendrocytes: a new resource for understanding brain development and function. *J Neurosci.* 2008; 28:264–78. [PubMed: 18171944]
- Ceelen PW, Lockridge A, Newman EA. Electrical coupling between glial cells in the rat retina. *Glia.* 2001; 35:1–13. [PubMed: 11424187]
- Coles JA, Orkand RK, Yamate CL, Tsacopoulos M. Free concentrations of Na, K, and Cl in the retina of the honeybee drone: stimulus-induced redistribution and homeostasis. *Ann N Y Acad Sci.* 1986; 481:303–17. [PubMed: 3468862]
- Connors BW, Long MA. Electrical synapses in the mammalian brain. *Annu Rev Neurosci.* 2004; 27:393–418. [PubMed: 15217338]
- D'Ambrosio R, Wenzel J, Schwartzkroin PA, McKhann GM 2nd, Janigro D. Functional specialization and topographic segregation of hippocampal astrocytes. *J Neurosci.* 1998; 18:4425–38. [PubMed: 9614220]
- Dermietzel R, Spray DC. Gap junctions in the brain: where, what type, how many and why? *Trends Neurosci.* 1993; 16:186–92. [PubMed: 7685944]
- Du Y, Ma B, Kiyoshi CM, Alford CC, Wang W, Zhou M. Freshly dissociated mature hippocampal astrocytes exhibit similar passive membrane conductance and low membrane resistance as syncytial coupled astrocytes. *J Neurophysiol.* 2015 jn 00206 2015.
- Furshpan EJ, Potter DD. Mechanism of nerve-impulse transmission at a crayfish synapse. *Nature.* 1957; 180:342–3. [PubMed: 13464833]
- Futamachi KJ, Pedley TA. Glial cells and extracellular potassium: their relationship in mammalian cortex. *Brain Res.* 1976; 109:311–22. [PubMed: 1276917]
- Gardner-Medwin AR, Nicholson C. Changes of extracellular potassium activity induced by electric current through brain tissue in the rat. *J Physiol.* 1983; 335:375–92. [PubMed: 6875884]
- Giaume C, Koulakoff A, Roux L, Holcman D, Rouach N. Astroglial networks: a step further in neuroglial and gliovascular interactions. *Nat Rev Neurosci.* 2010; 11:87–99. [PubMed: 20087359]
- Giaume C, Liu X. From a glial syncytium to a more restricted and specific glial networking. *J Physiol Paris.* 2012; 106:34–9. [PubMed: 21979115]

- Hesp ZC, Goldstein EA, Miranda CJ, Kaspar BK, McTigue DM. Chronic oligodendrogenesis and remyelination after spinal cord injury in mice and rats. *J Neurosci*. 2015; 35:1274–90. [PubMed: 25609641]
- Holthoff K, Witte OW. Directed spatial potassium redistribution in rat neocortex. *Glia*. 2000; 29:288–92. [PubMed: 10642755]
- Kettenmann H, Ransom BR. Electrical coupling between astrocytes and between oligodendrocytes studied in mammalian cell cultures. *Glia*. 1988; 1:64–73. [PubMed: 2853139]
- Khakh BS, McCarthy KD. Astrocyte calcium signaling: from observations to functions and the challenges therein. *Cold Spring Harb Perspect Biol*. 2015; 7:a020404. [PubMed: 25605709]
- Kimelberg HK. Functions of mature mammalian astrocytes: a current view. *Neuroscientist*. 2010; 16:79–106. [PubMed: 20236950]
- Kofuji P, Ceelen P, Zahs KR, Surbeck LW, Lester HA, Newman EA. Genetic inactivation of an inwardly rectifying potassium channel (Kir4.1 subunit) in mice: phenotypic impact in retina. *J Neurosci*. 2000; 20:5733–40. [PubMed: 10908613]
- Kofuji P, Newman EA. Potassium buffering in the central nervous system. *Neuroscience*. 2004; 129:1045–56. [PubMed: 15561419]
- Kuffler SW, Nicholls JG, Orkand RK. Physiological properties of glial cells in the central nervous system of amphibia. *J Neurophysiol*. 1966; 29:768–87. [PubMed: 5966434]
- Kuffler SW, Potter DD. Glia in the Leech Central Nervous System: Physiological Properties and Neuron-Glia Relationship. *J Neurophysiol*. 1964; 27:290–320. [PubMed: 14129773]
- Kuga N, Sasaki T, Takahara Y, Matsuki N, Ikegaya Y. Large-scale calcium waves traveling through astrocytic networks in vivo. *J Neurosci*. 2011; 31:2607–14. [PubMed: 21325528]
- Langer J, Stephan J, Theis M, Rose CR. Gap junctions mediate intercellular spread of sodium between hippocampal astrocytes in situ. *Glia*. 2012; 60:239–52. [PubMed: 22025386]
- Lin JH, Weigel H, Cotrina ML, Liu S, Bueno E, Hansen AJ, Hansen TW, Goldman S, Nedergaard M. Gap-junction-mediated propagation and amplification of cell injury. *Nat Neurosci*. 1998; 1:494–500. [PubMed: 10196547]
- Ma B, Xu G, Wang W, Enyeart JJ, Zhou M. Dual patch voltage clamp study of low membrane resistance astrocytes in situ. *Mol Brain*. 2014; 7:18. [PubMed: 24636341]
- Maldonado PP, Velez-Fort M, Levavasseur F, Angulo MC. Oligodendrocyte precursor cells are accurate sensors of local K<sup>+</sup> in mature gray matter. *J Neurosci*. 2013; 33:2432–42. [PubMed: 23392672]
- Meme W, Vandecasteele M, Giaume C, Venance L. Electrical coupling between hippocampal astrocytes in rat brain slices. *Neurosci Res*. 2009; 63:236–43. [PubMed: 19167439]
- Muller, CM. Gap-junctional communication in mammalian cortical astrocytes: development, modifiability and possible functions. In: Spary, DC.; Dermietzel, R., editors. *Gap Junctions in the nervous system*. Vol. Chapter 12. Austin, TX: RG Landes Company; 1996. p. 203–212.
- Nedergaard M, Ransom B, Goldman SA. New roles for astrocytes: redefining the functional architecture of the brain. *Trends Neurosci*. 2003; 26:523–30. [PubMed: 14522144]
- Newman EA. Regional specialization of retinal glial cell membrane. *Nature*. 1984; 309:155–7. [PubMed: 6717594]
- Newman EA. Propagation of intercellular calcium waves in retinal astrocytes and Muller cells. *J Neurosci*. 2001; 21:2215–23. [PubMed: 11264297]
- Newman EA, Frambach DA, Odette LL. Control of extracellular potassium levels by retinal glial cell K<sup>+</sup> siphoning. *Science*. 1984; 225:1174–5. [PubMed: 6474173]
- Nimmerjahn A, Kirchhoff F, Kerr JN, Helmchen F. Sulforhodamine 101 as a specific marker of astroglia in the neocortex in vivo. *Nat Methods*. 2004; 1:31–7. [PubMed: 15782150]
- Oakley B 2nd, Katz BJ, Xu Z, Zheng J. Spatial buffering of extracellular potassium by Muller (glial) cells in the toad retina. *Exp Eye Res*. 1992; 55:539–50. [PubMed: 1483500]
- Orkand RK, Nicholls JG, Kuffler SW. Effect of nerve impulses on the membrane potential of glial cells in the central nervous system of amphibia. *J Neurophysiol*. 1966; 29:788–806. [PubMed: 5966435]

- Ransom, BR. Do glial gap junctions play a role in extracellular ion homeostasis?. In: Spary, DC.; Dermietzel, R., editors. Gap Junctions in the nervous system. Austin, TX: RG Landes Company; 1996. p. 159-173.
- Ransom BR, Goldring S. Ionic determinants of membrane potential of cells presumed to be glia in cerebral cortex of cat. *J Neurophysiol.* 1973; 36:855–68. [PubMed: 4805015]
- Ransom BR, Kettenmann H. Electrical coupling, without dye coupling, between mammalian astrocytes and oligodendrocytes in cell culture. *Glia.* 1990; 3:258–66. [PubMed: 2144505]
- Rose CR, Ransom BR. Gap junctions equalize intracellular Na<sup>+</sup> concentration in astrocytes. *Glia.* 1997; 20:299–307. [PubMed: 9262234]
- Rouach N, Koulakoff A, Abudara V, Willecke K, Giaume C. Astroglial metabolic networks sustain hippocampal synaptic transmission. *Science.* 2008; 322:1551–5. [PubMed: 19056987]
- Simard M, Arcuino G, Takano T, Liu QS, Nedergaard M. Signaling at the gliovascular interface. *J Neurosci.* 2003; 23:9254–62. [PubMed: 14534260]
- Wallraff A, Kohling R, Heinemann U, Theis M, Willecke K, Steinhauser C. The impact of astrocytic gap junctional coupling on potassium buffering in the hippocampus. *J Neurosci.* 2006; 26:5438–47. [PubMed: 16707796]
- Wang F, Smith NA, Xu Q, Fujita T, Baba A, Matsuda T, Takano T, Bekar L, Nedergaard M. Astrocytes modulate neural network activity by Ca<sup>2+</sup>-dependent uptake of extracellular K<sup>+</sup>. *Sci Signal.* 2012; 5:ra26. [PubMed: 22472648]
- Xu G, Wang W, Kimelberg HK, Zhou M. Electrical coupling of astrocytes in rat hippocampal slices under physiological and simulated ischemic conditions. *Glia.* 2010; 58:481–93. [PubMed: 19795502]
- Xu G, Wang W, Zhou M. Spatial organization of NG2 glial cells and astrocytes in rat hippocampal CA1 region. *Hippocampus.* 2014; 24:383–95. [PubMed: 24339242]
- Zhang Y, Barres BA. Astrocyte heterogeneity: an underappreciated topic in neurobiology. *Curr Opin Neurobiol.* 2010; 20:588–94. [PubMed: 20655735]
- Zhou M, Schools GP, Kimelberg HK. Development of GLAST(+) astrocytes and NG2(+) glia in rat hippocampus CA1: mature astrocytes are electrophysiologically passive. *J Neurophysiol.* 2006; 95:134–43. [PubMed: 16093329]

**Main Points**

- Astrocytes are electrically coupled strongly with a coupling coefficient of 94%.
- The strong coupling equilibrates the membrane potentials among astrocytes to achieve a syncytial isopotentiality, whereby a constant chemical and quiescent electrical environment can be powerfully maintained.

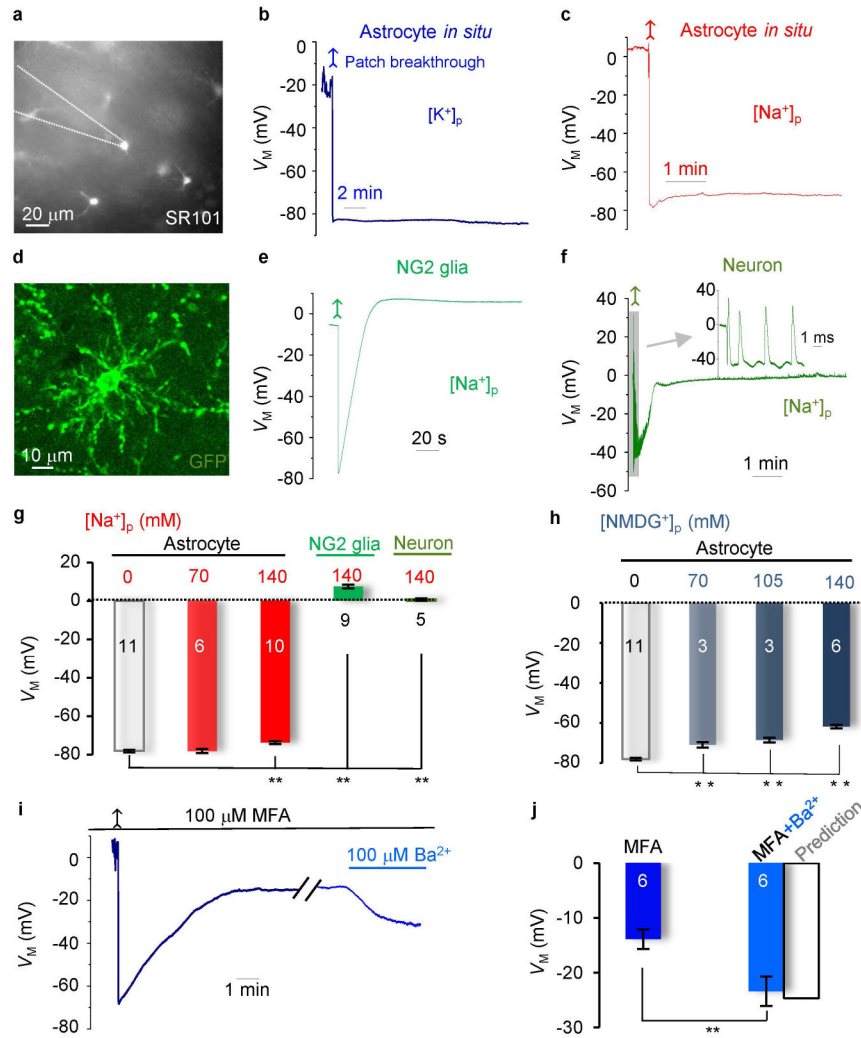


**Figure 1. Physiological  $V_M$  can be well-maintained in astrocyte recordings with reduced or  $K^+$  free pipette solutions *in situ***  
**(A)** SR101 staining of astrocytes in CA1 region. **(B and C)** Astrocyte  $V_M$  recordings, first in cell-attached, then in whole-cell mode after membrane patch breakthrough (arrows). The resting  $V_M$ 's were comparable between  $K^+_p$  and  $[Na^+]_p$  solutions. **(D and E)** An NG2 glia identified from PDGF-driven GFP transgenic mouse CA1 region *in situ*, and its  $V_M$  recording with  $[Na^+]_p$ . The  $V_M$  showed an initial hyperpolarization and a following depolarization. **(F)** The  $V_M$  recording from an interneuron with  $[Na^+]_p$ , showing an initially hyperpolarization ( $-40$  mV), followed by a depolarization ( $\sim 0$  mV). A burst of spikes appeared shortly after patch breakthrough (upper inset). **(G)** Summary of the  $V_M$  values for the cell types and conditions indicated (one-way ANOVA with post-hoc F test). **(H)** Summary of the  $V_M$  values from astrocytes recorded with various pipette NMDG<sup>+</sup> concentrations *in situ* (one-way ANOVA with post-hoc F test). **(I)** Gap junction inhibition by  $100 \mu\text{M}$  MFA depolarized  $V_M$  and the subsequent Kir4.1 inhibition ( $100 \mu\text{M}$  Ba<sup>2+</sup>) hyperpolarized  $V_M$  as predicted by the mathematical model (Supp. Info. Fig. 4). **(J)**

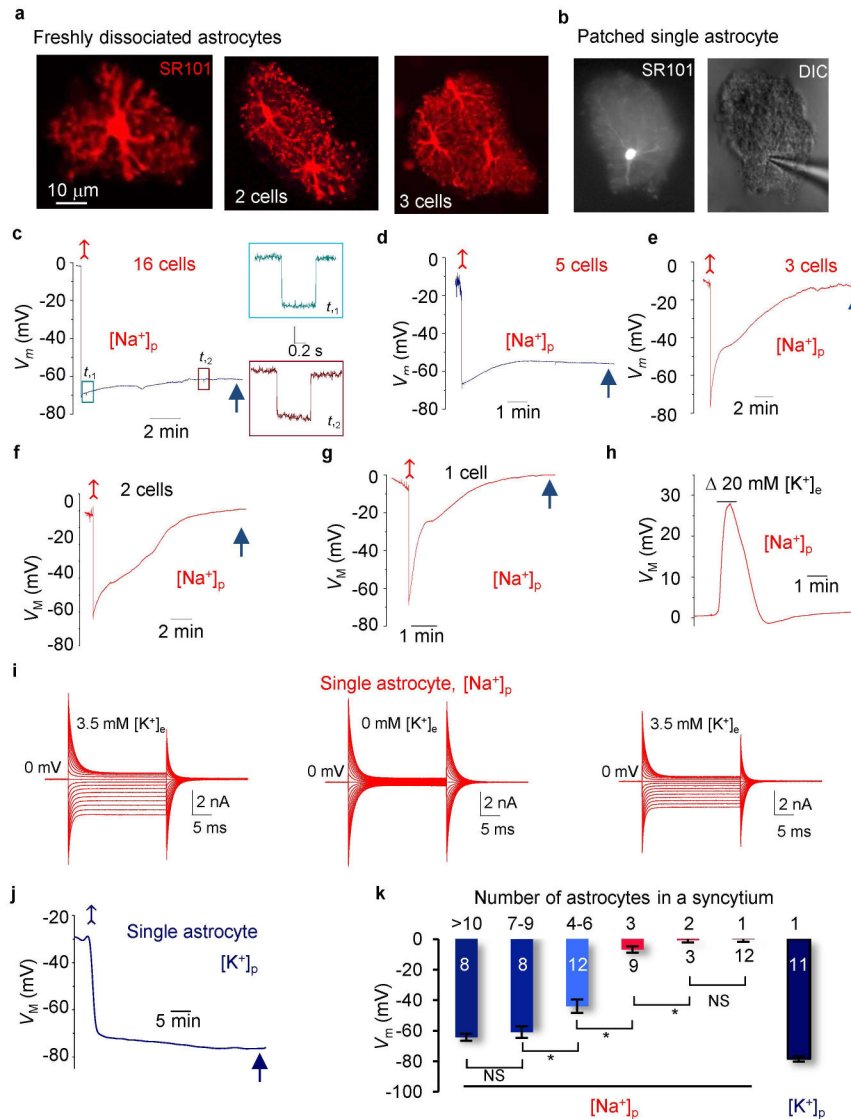
Summary of the  $V_M$  values in MFA, MFA+Ba<sup>2+</sup>, and a predicted value for the latter from the model (paired sample t test). \* $P < 0.05$ .

Author Manuscript

Author Manuscript

Author Manuscript

Author Manuscript



$V_M$  in  $[K^+]_p$  and  $[Na^+]_p$  pipette solutions (one-way ANOVA with post-hoc F test). \* $P < 0.05$ , *one way ANOVA* test.

Author Manuscript

Author Manuscript

Author Manuscript

Author Manuscript

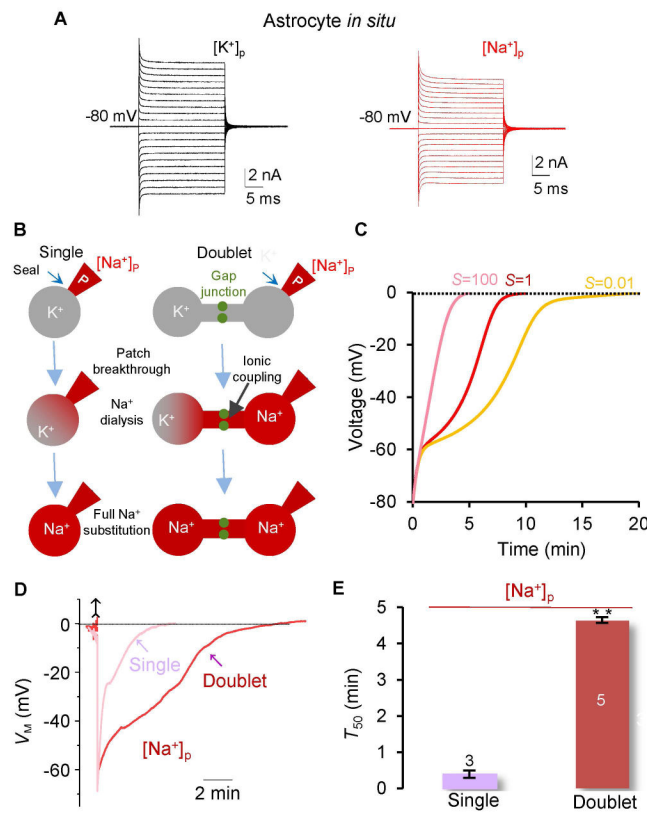


### Figure 3. The ion exchange efficacy at gap junction sites

(A) Representative  $V_M$  recordings from  $[K^+]_p$  and  $[Na^+]_p$  pipette solutions, as indicated *in situ*. (B) Schematic illustrations of Na<sup>+</sup> dialysis and substitution occurring in a single and a doublet astrocytes with a difference in the presence of gap junctional coupling in the latter. (C) Modeling predictions of the time courses for doublet astrocytes to reach to a full Na<sup>+</sup> substitution with different gap junction coupling strengths. The numerical 1 is the prediction for the highest ionic diffusion rate in a doublet; this predicts a time course that is most similar to that of a single cell. (D) The  $V_M$  recordings from single and doublet astrocytes with  $[Na^+]_p$  to determine their  $T_{50}$ 's. (E) The  $T_{50}$  values for Na<sup>+</sup> ion substitutions in single and doublet astrocytes (two sample t test). \*\* $P < 0.01$ , one way ANOVA test.

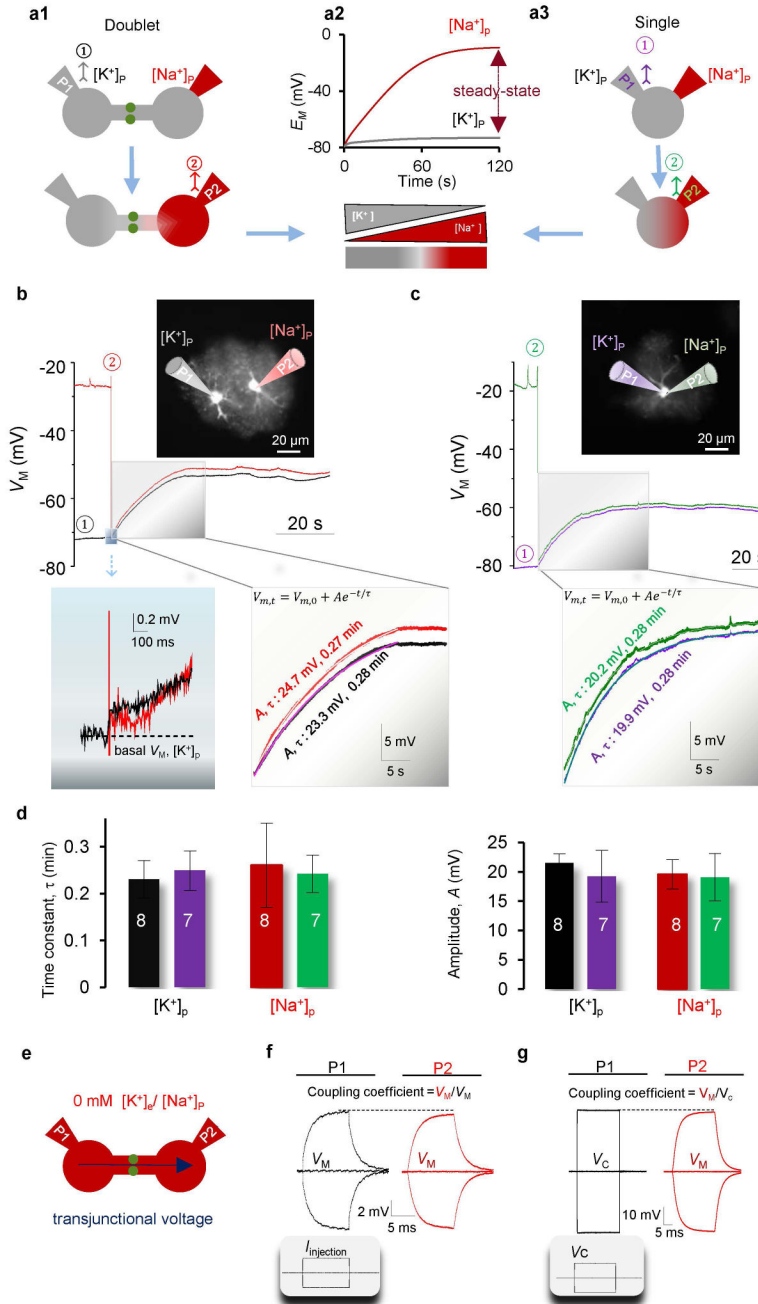


**Figure 4. Astrocyte doublets show equilibrated  $V_M$**

(A1) Schematic illustration of the recording procedure to achieve a separation of  $E_M$  in a doublet. The  $K^+$ -based electrode, P1, is ruptured first. This does not alter the  $[K^+]_i$  gradient, but enables the reading of  $V_M$ . (A2) The model prediction of  $E_M$  separation between P1 and P2 during  $Na^+$ -dialysis and at the steady-state levels. (A3) Similar to a1 to separate the  $E_M$  in a single astrocyte at P1 and P2. (B–C) The  $V_M$  recordings from a doublet (B) and a single astrocyte (C) following the procedure described in a. Each trace is color coded with its corresponding recording pipette (P). In a doublet, the initial  $V_M$ , just after the breakthrough of P2, is shown in expanded scale to disclose the immediate equilibration of  $V_M$  in both

cells. In both doublet and single astrocyte, the progression of  $V_M$  to the steady-state levels are shown in expanded scale (middle and right insets, respectively). Each trace was superimposed with a single exponential fit in order to determine a time constant ( $\tau$ ) and  $V_M$  amplitude. **(D)** The derived  $\tau$ 's and the  $V_M$  amplitudes among the four pipettes. **(E)** Illustration of the use of  $K^+$  free solutions to maximally reduce the transjunctional voltage and allow for accurate measurement of the coupling coefficient (CC) and gap junction resistance ( $R_g$ ) (one-way ANOVA with post-hoc F test). **(F-G)** The respective current clamp **(F)** and combined voltage and current clamp **(G)** recording modes for measurement of CC and  $R_g$ , as indicated. The access resistance ( $R_a$ ) was not compensated for the delivered  $V_C$  in P1**(G)**. The resulting strong CC and low  $R_g$  indicate that doublets electrically behave as single astrocytes.

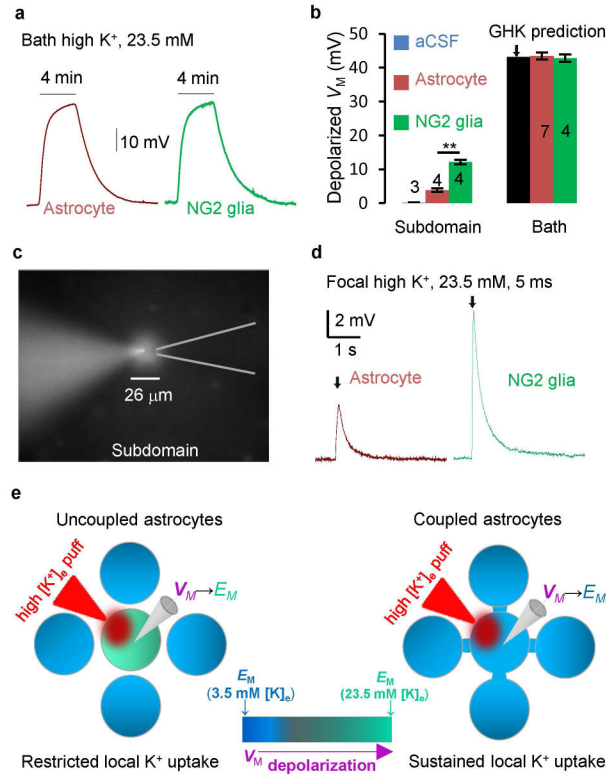


**Figure 5. Synctial coupling attenuates local elevated extracellular  $K^+$ -induced  $V_M$  depolarization**

(A) Bath 23.5 mM high  $K^+$ -induced  $V_M$  depolarization from an astrocyte and an NG2 glia, as indicated. (B) Summary of bath and local high  $[K^+]_e$  induced  $V_M$  depolarization. (C) A 5 ms local high  $[K^+]_e$  was applied to a recorded astrocyte with an affected subdomain area monitored by SR101 included in the high  $[K^+]_e$  solution (two sample t test). (D) A 5 ms local high  $[K^+]_e$  puff induced  $V_M$  depolarization in an astrocyte and an NG2 glia. (E) Schematic illustration of  $V_M$  response to a high  $[K^+]_e$  puff. In an uncoupled astrocyte, the  $V_M$  quickly depolarizes to the new elevated  $[K^+]_e$  established  $E_M$ . Once  $V_M \rightarrow E_M$ , the  $K^+$  uptake stops. In coupled astrocytes, the  $V_M$  remains close to a constant. This maintains the driving force,  $V_M - E_M$ , for a “sustained  $K^+$  uptake”. \* $P < 0.05$ , one way ANOVA test for comparison of the  $V_M$  depolarization between astrocytes and NG2 glia.